LAWRENCE
LIVERMORE
NATIONAL
LABORATORY

UCRL-JRNL-218773

Accurate Astrometry and Photometry of Saturated and Coronagraphic Point Spread Functions

C. Marois, D. Lafreniere, B. Macintosh, R. Doyon

February 8, 2006

Astrophysical Journal

Accurate Astrometry and Photometry of Saturated and Coronagraphic Point Spread Functions

Christian Marois[1], David Lafrenière[2], Bruce Macintosh[1] & René Doyon[2]

[1] *Institute of Geophysics and Planetary Physics L-413,*
Lawrence Livermore National Laboratory, 7000 East Ave, Livermore, CA 94550

[2] *Département de physique and Observatoire du Mont Mégantic, Université de Montréal,*
C.P. 6128, Succ. A,
Montréal, QC, Canada H3C 3J7

cmarois@igpp.ucllnl.org david@astro.umontreal.ca bmac@igpp.ucllnl.org
doyon@astro.umontreal.ca

ABSTRACT

For ground-based adaptive optics point source imaging, differential atmospheric refraction and flexure introduce a small drift of the point spread function (PSF) with time, and seeing and sky transmission variations modify the PSF flux. These effects need to be corrected to properly combine the images and obtain optimal signal-to-noise ratios, accurate relative astrometry and photometry of detected companions as well as precise detection limits. Usually, one can easily correct for these effects by using the PSF core, but this is impossible when high dynamic range observing techniques are used, like coronagrahy with a non-transmissive occulting mask, or if the stellar PSF core is saturated. We present a new technique that can solve these issues by using off-axis satellite PSFs produced by a periodic amplitude or phase mask conjugated to a pupil plane. It will be shown that these satellite PSFs track precisely the PSF position, its

Strehl ratio and its intensity and can thus be used to register and to flux normalize the PSF. This approach can be easily implemented in existing adaptive optics instruments and should be considered for future extreme adaptive optics coronagraph instruments and in high-contrast imaging space observatories.

Subject headings: Instrumentation: AO - planetary systems - stars: imaging

Suggested running page header: Accurate PSF Astrometry and Photometry

1. Introduction

Ground-based adaptive optics, both standard observing techniques and more specialized observing methods aimed for high-contrast imaging, like simultaneous spectral differential imaging (Racine et al. 1999; Marois et al. 2000; Biller et al. 2004; Marois 2004; Marois et al. 2005), angular differential imaging (Marois 2004; Liu 2004; Marois et al. 2006) and coronagraphy (Lyot 1932), generally require the acquisition of a long sequence of images. The object airmass, the telescope orientation and the observing conditions (seeing and sky transmission) change during the sequence, producing point spread function (PSF) flux and Strehl ratio variations over time. The PSF is also slowly moving in time due to flexure and differential atmospheric refraction if a near-infrared camera is used while operating the adaptive optics wavefront sensor in the visible. If not corrected, these effects bias the relative photometry and astrometry of sources detected in the field of view (FOV) and the estimated detection limits. To obtain the optimal signal-to-noise ratio (S/N) and precise astrometry and photometry after combination of all acquired images, each individual image needs to be accurately registered and flux normalized.

Standard techniques to register a PSF and estimate the relative astrometry of sources detected in the FOV require the information from PSF core. If the PSF core is saturated to

improve observing efficiency or if a non-transmissive focal plane occulter is used, the PSF core is not visible and other techniques need to be applied. If available, an off-axis sharp ghost image can be used to register the PSF and estimate its core position, but the possibility of a non-common motion between the ghost and the PSF makes the registering uncertain.

The usual technique to estimate detection limits (or a source relative intensity) when the PSF core is saturated or occulted is to compare the noise in the combined image (or a source peak intensity) to the peak intensity of an unsaturated/unocculted PSF acquired before and/or after the saturated/occulted image sequence. Such estimates can be biased by the short exposure time and small number of images that are considered when acquiring unsaturated/unocculted data. Furthermore, the observing conditions of the unsaturated/unocculted images can be significantly different from those of the saturated/occulted image sequence.

To obtain the highest S/N ratio in the combined image, one would want, ideally, to normalize the images such that any point source, after image registration, has the same number of counts per full width at half maximum (FWHM) in each image. The images would then be weighted by the inverse square of their noise and combined.

A simple solution to these astrometric and photometric problems exist. A periodic phase or amplitude mask can be introduced at a pupil plane to produce fainter off-axis copies of the primary PSF. The position and relative intensity of these satellite PSFs are fixed by the mask amplitude and spatial frequency. These satellite PSFs track precisely the PSF core position as well as its intensity variations. They can thus be used for accurate astrometry and photometry. First, this technique will be analyzed using a simple analytical model and numerical simulations. The technique will then be illustrated using a laboratory experiment. A technique similar to the one presented in this paper has been independently developed by Sivaramakrishnan & Oppenheimer (2006).

2. Non-Coronagraphic PSFs

The effect of a pupil-plane conjugated aberration can be estimated using a far-field approximation. The intensity $I(\eta, \xi)$, where η and ξ are coordinates in the focal plane, of the PSF is simply the Fourier transform FT of the complex electric field (Schroeder 1987) at the pupil

$$I(\eta, \xi) = \left|\mathrm{FT}(\mathrm{A(x,y)e^{i[\phi(x,y)]}})\right|^2 = |F_a|^2 = I_a \tag{1}$$

where A is the wavefront amplitude, equal to one inside the pupil and zero elsewhere, and ϕ its phase, having a noise RMS σ inside the pupil. Both A and ϕ are expressed in coordinates x and y in the pupil and are real functions. The phase ϕ has zero mean. The functions I_a and F_a are respectively the aberrated PSF intensity and its complex focal plane electric field. The next two sub-sections will study the effect of adding a specific phase or amplitude pupil-plane mask to the aberrated wavefront. It is assumed in the following analysis that $\phi(x, y)$ is small, i.e. space-based imaging or partially corrected by an AO system, producing diffraction limited images.

2.1. Pupil-Plane Periodic Phase Mask

If a phase aberration ϕ_{mask} having a FT equal to Φ_{mask} and a standard deviation of σ_{mask} is introduced on the wavefront at a pupil plane, the effect on the intensity of the PSF can be deduced from Eq. 1. The aberration Φ is simply replaced by $\Phi + \Phi_{\mathrm{mask}}$ and the following expression is found

$$I(\eta, \xi) = \left|\mathrm{FT}(\mathrm{A(x,y)e^{i[\phi(x,y)+\phi_{mask}(x,y)]}})\right|^2 \tag{2}$$

Separating the effect of the mask, we find

$$I(\eta,\xi) = \left|\mathrm{FT}([\mathrm{A(x,y)e^{i[\phi(x,y)]}}][\mathrm{e^{i[\phi_{mask}(x,y)]}}])\right|^2 \tag{3}$$

Following the work of Bloemhof et al. (2001); Sivaramakrishnan et al. (2002); Perrin et al. (2003), assuming ϕ_{mask} is small, the complex exponential of ϕ_{mask} can be expanded using a Taylor approximation to find

$$I(\eta,\xi) \cong \left|\mathrm{FT}([\mathrm{A(x,y)e^{i[\phi(x,y)]}}][1 + \mathrm{i}\phi_{\mathrm{mask}} - \frac{\phi^2_{\mathrm{mask}}}{2} + \ldots])\right|^2 \tag{4}$$

Keeping only terms up to the second order and using the fact that the Fourier transform of a product is the convolution of the Fourier transform of the two terms, we find

$$I(\eta,\xi) \cong I_a + 2\Im[F_a^*(F_a \star \Phi_{\mathrm{mask}})] - \Re[F_a^*(F_a \star \Phi_{\mathrm{mask}} \star \Phi_{\mathrm{mask}})] + |F_a \star \Phi_{\mathrm{mask}}|^2 \tag{5}$$

If the phase mask is chosen to be a periodic function, Φ_{mask} is sharply peaked at symmetric locations. The term $F_a \star \Phi_{\mathrm{mask}}$ thus simply add replicas of F_a at each peak of Φ_{mask}. For the replicas to be greater than I_a at the same separation, σ_{mask} needs to be larger than the noise component of σ at the spatial frequency corresponding to the mask periodicity. Since both the second and third terms are multiplied by F_a, a function that sharply drop to zero with angular separation for diffraction limited images, they can be neglected. In that case, the fourth term dominates and we find that the PSF intensity evolution due to the phase mask is simply

$$I(\eta,\xi) - I_a \cong |F_a \star \Phi_{\mathrm{mask}}|^2 \tag{6}$$

Since F_a is the aberrated PSF electric field, the periodic phase mask produces replicas of the aberrated PSF, we call these satellite PSFs. Since the satellite PSFs are produced by a convolution of the aberrated PSF, they track the PSF core position and intensity variations. The intensity and location of the satellite PSFs are respectively set only by the amplitude and periodicity of the phase mask, they are thus insensitive to a mask offset.

If we assume that the phase mask is a sine wave, two satellite PSFs will be produced at an angular separation equal to the number of cycles per pupil in λ/D units and with a relative intensity equal to $\sigma^2_{\rm mask}/2$. Fig. 1 shows an unaberrated 1.6 μm monochromatic PSF with a 30 nm amplitude sine wave phase mask having 25 cycles per pupil as well as a PSF having the same sine wave phase mask but with a 150 nm RMS phase aberration having a power spectral density (PSD) following a power-law of index -2.6. PSFs are simulated with a 256 pixels diameter circular pupil inside a 1024 $\times$ 1024 pixels image producing a PSF having 4 pixels per λ/D. The satellite PSFs are clearly symmetric and track the PSF position, Strehl ratio and its intensity. These satellite PSFs can thus be used for registering and photometric calibration (see sect. 4).

2.2. Pupil-Plane Periodic Amplitude Mask

A similar analysis can be done for pupil plane conjugated aberrations. Introducing an amplitude mask $\epsilon_{\rm mask}$ having a FT equal to $E_{\rm mask}$ and a standard deviation $\sigma_{\rm mask}$ on the wavefront conjugated to the pupil plane modifies Eq. 1 as follows

$$I(\eta,\xi) = |{\rm TF}([{\rm A} + {\rm A}\epsilon]{\rm e}^{{\rm i}[\phi({\rm x,y})]})|^2 \tag{7}$$

Reorganizing this equation, we find

$$I(\eta,\xi) = [\mathrm{TF}(\mathrm{Ae}^{\mathrm{i}[\phi(\mathrm{x,y})]}) + \mathrm{TF}([\mathrm{A}\epsilon]\mathrm{e}^{\mathrm{i}[\phi(\mathrm{x,y})]})][\mathrm{TF}(\mathrm{Ae}^{\mathrm{i}[\phi(\mathrm{x,y})]}) + \mathrm{TF}([\mathrm{A}\epsilon]\mathrm{e}^{\mathrm{i}[\phi(\mathrm{x,y})]})]^* \tag{8}$$

Knowing that the FT of a multiplication is the convolution of the two FTs, we thus find

$$I(\eta,\xi) = I_a + 2\Re[F_a(F_a^* \star E^*)] + |F_a \star E|^2 \tag{9}$$

Following the argument of section 2.1, the second can be neglected and we find the intensity modification from the added mask

$$I(\eta,\xi) - I_a \cong |F_a \star E|^2 \tag{10}$$

The satellite PSFs are thus again copies of the primary aberrated PSF.

If the amplitude mask is a sine wave, the satellite PSFs have a relative intensity equal to $\sigma^2_{\mathrm{mask}}/2$ and their separation is equal to the number of cycles per pupil in λ/D units. Fig. 2 shows an unaberrated 1.6 μm monochromatic PSF with a 12% amplitude sine wave transmission mask having 25 cycles per pupil as well as an aberrated PSF with the same sine wave mask but with 150 nm RMS phase aberration as in section 2.1. Similarly to what has been found for a phase mask, the satellite PSFs track the PSF core position and its intensity.

Instead of a sine wave amplitude mask, another option is to simply use a transmission amplitude grating consisting of wires to mask a periodic section of the pupil. In that case, Eq. 10 is still valid and the satellite PSFs will be the convolution of the wire grid (transmission step function) Fourier transform with the aberrated PSF. The wire grid can be treated as a multi-slit Young experiment and the satellite PSFs intensity function I^s is thus simply (Hecht 1998)

$$I^s(\theta) = I_0^s \left(\frac{\sin\beta}{\beta}\right)^2 \left(\frac{\sin N\alpha}{\sin\alpha}\right)^2 \tag{11}$$

where θ is the angular separation along the satellite PSFs axis, I_0^s is the intensity at $\theta = 0$, N is the number of wires accross the pupil and β and α are respectively equal to $(kb/2)\sin\theta$ and $(ka/2)\sin\theta$. The constant k is the propagation number $(2\pi/\lambda)$ and the values a and b are respectively the wire spacing and thickness. The first parenthesis in Eq. 11 is the intensity enveloppe produced by the diffraction of a single wire (sinc function having $\sim \lambda/b$ FWHM) while the second parenthesis is an intensity modulation from the interference of diffracted light from all wires. Satellite PSFs (local maxima) appear at $m\lambda/a$ separation, where m is an integer. In contrast to the phase and amplitude sine wave masks that show two symmetric satellite PSFs, the transmission amplitude grating produces numerous satellite PSFs. The relative intensity, at $\theta = 0$, of the satellite PSFs is equal to the square of the ratio of the area masked by the grating over that in the unobscured pupil region

$$\frac{I_0^s}{I_0} = \left(\frac{\int_{\text{Pupil}}(A\epsilon)dxdy}{\int_{\text{Pupil}}(A + A\epsilon)dxdy}\right)^2 \tag{12}$$

where I_0 is the aberrated PSF peak intensity. For a uniform pupil having numerous wires, the intensity ratio can be approximated by

$$\frac{I_0^s}{I_0} \cong \left(\frac{b}{a-b}\right)^2. \tag{13}$$

If $a \gg b$, the ratio is simply $(b/a)^2$.

Fig. 3 shows an unaberrated 1.6 μm monochromatic PSF simulation with a 25 cycle per pupil grating having wires of width equal to 1/250, as well as an aberrated PSF (150 nm RMS phase aberration) with the same grating. The added speckles again track the PSF position, Strehl ratio and its intensity (see Sect. 4).

3. Coronagraphic PSFs with added phase/amplitude mask

The analysis presented in Sect. 2 was done using a far field approximation without the use of a coronagraph. If a coronagraph is used, the amplitude/phase mask needs to be introduced before the focal plane occulter so that the satellite PSFs be replicas of the unocculted PSF. If we consider a simple pupil plane Gaussian apodizer, it is easy to understand from Eq. 6 and Eq. 10 that the conclusion of Sect. 2 is still valid for a coronagraph since PSFs are simply obtained with A being the apodized pupil instead of a uniform pupil. A Gaussian apodized pupil for a 1.6 μm monochromatic PSF was simulated using the transmissive amplitude grating with and without 150 nm RMS phase aberration (see Fig. 4) to simulate a coronagraphic PSF. The apodized coronagraph was chosen here since the PSF diffraction core is still detectable and can be used to verify that satellite PSFs track the PSF core position and its intensity. The result would be the same for a band-limited (Kuchner & Traub 2002) or a standard Lyot coronagraph since the grating is introduced in a pupil plane before the focal plane mask occulter and because, similarly to the apodized pupil coronagraph, these coronagraphs produce PSFs which are dominated by the second order halo term (Perrin et al. 2003; Bloemhof 2004). The simulation confirms that the satellite PSFs do again track the PSF core position and intensity.

4. Expected Astrometric and Photometric precision

In previous sections, it was shown that periodic amplitude or phase masks can be used for astrometry and photometry of saturated and coronagraphic PSFs. In realistic conditions, the satellite PSFs are overlaid over a background of speckle noise that can affect the determination of the satellite PSFs centers and intensities. It is thus important to adjust the intensity of the satellites PSFs to ensure that the desired accuracy is realized. Numerical simulations are now used to analyze the centering and relative intensity precisions of the

technique. Each satellite PSF is cross-correlated with a Gaussian to determine its precise location. The average X and Y positions of two symmetric satellite PSFs are then used to derive the PSF center. This derived position is then compared to the calculated PSF center using the same cross-correlation algorithm on the PSF core. Relative intensities are simply obtained by taking the ratio of the satellite's peak intensity over that of the primary PSF. Twenty simulations using independent 150 nm RMS phase aberrations were realized for amplitude sine, phase sine and amplitude grating masks for both cases with and without the Gaussian apodized pupil. For these simulations, masks were introduced in the pupil plane and satellite PSFs were 1000 times brighter than the local speckle noise. Table 1 summarizes the registering and relative intensity precisions. Typically, an error of 0.1 pixels RMS (1/40 λ/D) is found for both the non-coronagraph and the coronagraph cases. Typical relative intensities are precise to less than $\sim$2%, enough for accurate flux normalization.

Table 2 presents the registering precision for the non-coronagraph and coronagraph cases using the transmissive amplitude grating at the pupil plane for different satellite PSF intensities relative to the local speckle noise. Satellite PSFs 10 times brighter than the speckle noise limit the PSF registering accuracy to 1 pixel RMS (1/4 λ/D) and the photometric calibration to 20-30%, while satellite PSFs being 1000 times brigther than the background speckle noise limit the PSF registering to 0.1 pixels RMS (1/40 λ/D) and the photometric calibration to 2%. A satellite PSF relative intensity of $\sim$ 100 times the background speckle noise seems to be a good choice to avoid over-luminous satellite PSFs while offering good registering and photometric accuracies (0.3 pixel RMS (1/10 λ/D) and 5%). Such an astrometric precision is sufficient to confirm proper motion of nearby systems (typically 0.01 to 0.1 arcsec/year) in one year (diffraction limited H-band images acquired with a 10-m telescope).[1] Due to detector dynamic range limits, to minimize satellite PSF intensities, it might

[1]For speckle noise limited companion detections, the derived astrometric precisions from Sect. 4 simula-

be more convenient to use a large number of fainter satellite PSFs to average the speckle noise bias, albeit at the cost of a greater FOV contamination, or choose a mask frequency to move the satellite PSFs to wide separations, where the speckle noise is generally smaller.

5. Laboratory Experiment

A transmissive amplitude grating has been tested on the Université de Montréal high contrast imaging testbed. Commercial lenses were used to make a f/31 imaging system, yeilding, at 1.625 μm, a PSF having 2.7 pixels per λ/D. The pupil diameter was 13.1 mm. A transmissive amplitude grating mask having 150 ± 10 μm thick wires and 595 ± 15 μm spacing was introduced 10 mm from the pupil plane. This slight defocus was necessary due the mask and pupil stop mounts. The geometric pupil diameter at the grating mask conjugated plane is calculated to be 12.75 mm. With this setup, the diffraction envelope of a single wire drops to 0.97 of its peak at a separation of 17.1 λ/D, the location of the first satellite PSF. It is thus expected that this grating will produce satellite PSFs having a relative intensity of $0.97 \times (150/595)^2 = 0.062 \pm 0.012$ at 17.1 ± 0.5 λ/D separation. The pinhole was moved and an aberration phase plate was introduced in the beam to confirm that these satellite PSFs do track the PSF core position and intensity. All acquired images were unsaturated and reduced by subtracting a dark frame and divinding by a flat field. Fig. 5 shows the resulting PSFs. Satellite PSFs have a relative intensity of 0.058 and are situated at 16.8 λ/D from the PSF center, both values being consistent to the calculated values to 1σ accuracy, and track the PSF core position and intensity, in agreement with what was expected. In all above experiments, it was possible to register the PSF to less than 0.1

---

tions also mean that companions need to be at least 100 times brigther than the background speckle noise to obtain 1/10 λ/D center determination accuracy and allow their proper motion follow-up in one year for typical nearby systems - fainter companions will require a bigger time interval or longer integration time.

pixel precision (1/30 λ/D) with the average position of two symmetric satellite PSFs.

6. Discussion

Simulations presented in this paper are monochromatic. If a wide bandpass is used instead, satellite PSFs will be fainter relative to the core and elongated. Additionally, for ground-based imaging, if no atmospheric dispersion corrector is used, the elongation of the satellite PSFs will not necessarily point to the PSF center due to differential atmospheric refraction between the blue and red side of the bandpass. However, the midpoint of the line connecting the centers of opposite satellite PSFs still coincides with the PSF center.

Distortions coming from optics after the added mask can change the relative position of the satellite PSFs. Astrometric position of the satellite PSFs will thus need to be calibrated using an internal source or on-sky observations. To obtain precise relative astrometry of detected companions, distortion corrections for the entire optical system is also required.

The satellite PSFs will occupy a small portion of the FOV. Once the PSF is registered and flux normalized, they could be removed to avoid masking faint sources. Since the angular separation and size of the satellite PSFs is chromatic and fixed with respect to the instrument, a simple solution to remove them while conserving the flux of nearby sources would be to use the simultaneous spectral differential imaging SSDI (Racine et al. 1999; Marois et al. 2000; Biller et al. 2004; Marois et al. 2005) and/or the angular differential imaging techniques ADI (Marois 2004; Liu 2004; Marois et al. 2006).

If we consider the Gemini Altair AO system (Herriot et al. 1998) and NIRI near-infrared camera (Hodapp et al. 2000) for a possible implementation, satellite PSFs $\sim$ 10 magnitudes fainter that the central peak and located at a separation of 4 arcsec (100 λ/D in H-band) should be $\sim$100 times brighter the local speckle noise (Marois et al. 2006). If we put the

grating just in front of Altair's deformable mirror, where the wavefront diameter is 84 mm, a wire spacing and thickness of 0.832 mm an 8 μm would respectively be required. For very high contrast imaging aiming for detection limits better than 20 magnitudes at less than 1 arcsec, wire thickness will become an issue. A potential solution is to place the satellite PSFs at 5 λ/D. Using the same 8 μm thick wires and wavefront diameter as the above example, it would produce satellite PSFs that are 16.5 magnitudes fainter then the primary. Another solution is to generate satellite PSFs using a small phase periodic aberrations using the deformable mirror or phase plate.

7. Conclusion

It was shown both analytically and numerically that periodic amplitude and phase masks conjugated to the pupil plane can be used to produce satellite PSFs that track the PSF core position and intensity. Satellite PSFs being 100 times brigther than the speckle noise achieve registering and photometric accuracies of 0.3 pixels RMS (1/10 λ/D) and 5% respectively. Such precisions are sufficient to properly combine images and to confirm proper motion of nearby systems within one year when using diffracted limited H-band images from a 10-m telescope. Once the PSF is registered and flux normalized, these satellite PSFs can be removed to avoid FOV contamination by using the SSDI and/or ADI imaging techniques.

As demonstrated by the laboratory experiment, this technique can be easily implemented by using a transmissive amplitude grating. The laboratory experiment has confirmed that an amplitude mask conjugated to the pupil plane produces such satellite PSFs and that they do track the PSF core position and intensity while demonstrating the simplicity of the technique.

This technique could play an important role in next generation extreme adaptive optics

coronagraph systems like the Gemini Planet Imager (Macintosh et al. 2003, 2006) or the VLT Planet Finder (Mouillet et al. 2004) as well as in future high contrast coronagraphic space observatories.

Authors would like to thank Anand Sivaramakrishnan for stimulating discussions. This research was performed under the auspices of the US Department of Energy by the University of California, Lawrence Livermore National Laboratory under contract W-7405-ENG-48, and also supported in part by the National Science Foundation Science and Technology Center for Adaptive Optics, managed by the University of California at Santa Cruz under cooperative agreement AST 98-76783. This work is supported in part through grants from the Natural Sciences and Engineering Research Council, Canada and from the Fonds Québécois de la Recherche sur la Nature et les Technologies, Québec.

REFERENCES

Biller, B. A., Close, L.,Lenzen, R., Brandner, W., McCarthy, D., Nielsen, E., Hartung, M. 2004, Proc. SPIE, 5490, 389

Bloemhof, E. E., Dekany, R. G., Troy, M., Oppenheimer, B. R. 2001, ApJL, 558, L71

Bloemhof, E. E. 2004, ApJ, 610, L69

Hecht, E. 1998, "Optics", third edition, Addison Wesley Longman, Inc. 693 pages.

Herriot, G., Morris, S., Roberts, S., Fletcher, J. M., Saddlemyer, L. K., Singh, G., Veran, J., Richardson, E. H. 1998, Proc. SPIE, 3353, 488

Hodapp, K., Hora, J., Graves, E., Irwin, E. M., Yamada, H., Douglass, J. W., Young, T. T., Robertson, L. 2000, Proc. SPIE, 4008, 1334

Kuchner, M. J., & Traub, W. A. 2002, ApJ, 570, 900

Liu, M. C. 2004, Science, 305, 1442

Lyot, B. 1932, Zeitschrift fur Astrophysics, 5, 73

Macintosh, B. A., Becklin, E. E., Kaisler, D, Konopacky, Q., Zuckerman, B. 2003, ApJ, 594, 538

Macintosh, B., et al 2006 Proc. SPIE, 6113, 08

Marois, C. 2004, PhD. thesis, Université de Montréal

Marois, C., Doyon, R., Racine, R. & Nadeau, D. 2000 PASP, 112, 91

Marois, C., Doyon, R., Racine, R., Nadeau, D., Riopel, M., Vallée, P., Lafrenière, D. 2005 PASP, 117,745

Marois, C., Lafrenière, D., Doyon, R., Nadeau, D. 2006, ApJ, in press (astro-ph/0512335)

Mouillet, D., Lagrange, A. M., Beuzit, J.-L., Moutou, C., Saisse, M., Ferrari, M., Fusco, T., Boccaletti, A. 2004, ASP Conf. Ser., 321, 39

Perrin, M. D., Sivaramakrishnan, A., Makidon, R. B., Oppenheimer, B. R., Graham, J. R. 2003, ApJ, 596, 702

Racine, R., Walker, G. A. H., Nadeau, D., Doyon, R., Marois, C. 1999, PASP, 111, 587

Schroeder, D. J. "Astronomical Optics", San Diego: Academic Press, 1987

Sivaramakrishnan, A., Lloyd, J. P., Hodge, P. E., Macintosh, B. A. 2002, ApJL, 581, 59

Sivaramakrishnan, A., Oppenheimer, B. 2006, ApJ, submitted.

Table 1: PSF registering and flux normalizing precision.

Aberration	Coro.	With 150nm RMS	dx rms (pixel)	dy rms (pixel)	$I_{\rm satel}/I_{\rm PSF}$	$I_{\rm satel}/I_{\rm PSF}$ rms	$I_{\rm satel}/I_{\rm PSF}$ expected
Phase	no	no	-	-	0.00699	-	0.00694
Phase	no	yes	0.06	0.04	0.00686	0.00029	0.00694
Phase	yes	yes	0.08	0.07	0.00686	0.00042	0.00694
Amplitude	no	no	-	-	0.00695	-	0.00694
Amplitude	no	yes	0.09	0.07	0.00697	0.00015	0.00694
Amplitude	yes	yes	0.11	0.15	0.00694	0.00022	0.00694
Grid	no	no	-	-	0.01197	-	0.01000
Grid	no	yes	0.08	0.03	0.01199	0.00010	0.01235
Grid	yes	yes	0.10	0.13	0.01237	0.00019	0.01235

Table 2: Speckle intensities vs PSF registering and flux normalizing precision.

Speckle Intensity ratio	Coro.	dx rms	dy rms	$I_{\rm satel}/I_{\rm PSF}$	$I_{\rm satel}/I_{\rm PSF}$ (rms)
10	no	0.52	0.75	0.00014	0.00003
10	yes	1.00	1.11	0.00017	0.00005
100	no	0.22	0.18	0.00122	0.00006
100	yes	0.22	0.29	0.00152	0.00010
1,000	no	0.06	0.05	0.01203	0.00020
1,000	yes	0.07	0.09	0.01504	0.00029
10,000	no	0.02	0.02	0.12000	0.00049
10,000	yes	0.03	0.02	0.15007	0.00066

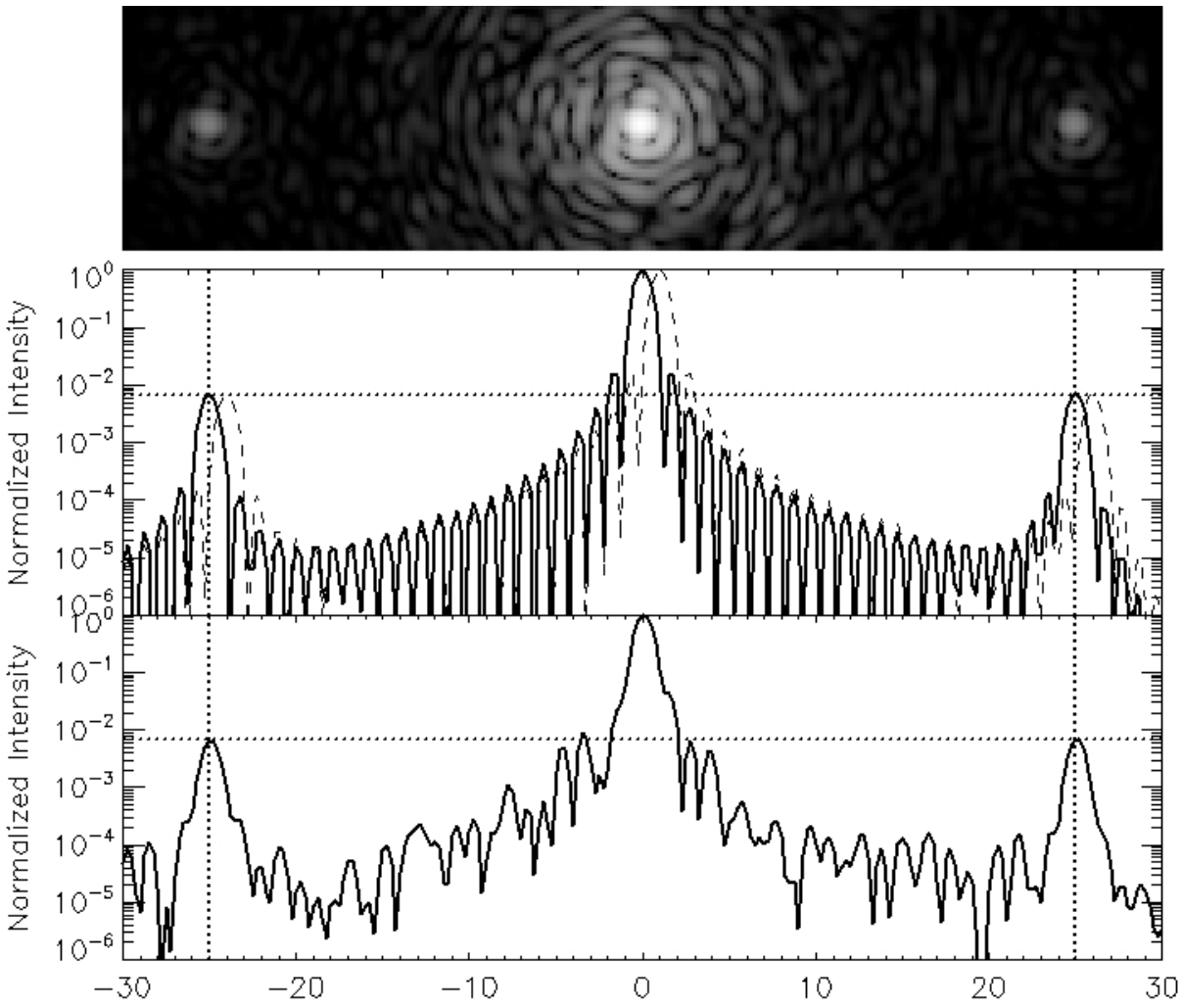

Fig. 1.— Central plot: Simulated monochromatic PSF with added sine wave phase mask (solid line). The dashed line shows the same simulation with an added tilt to show that the satellite PSFs track the PSF core position. Top panel and bottom plot: the same simulation with an added 150 nm RMS phase aberration. Dotted lines show the satellite PSFs expected positions and intensities. Top panel is shown on a logarithmic scale.

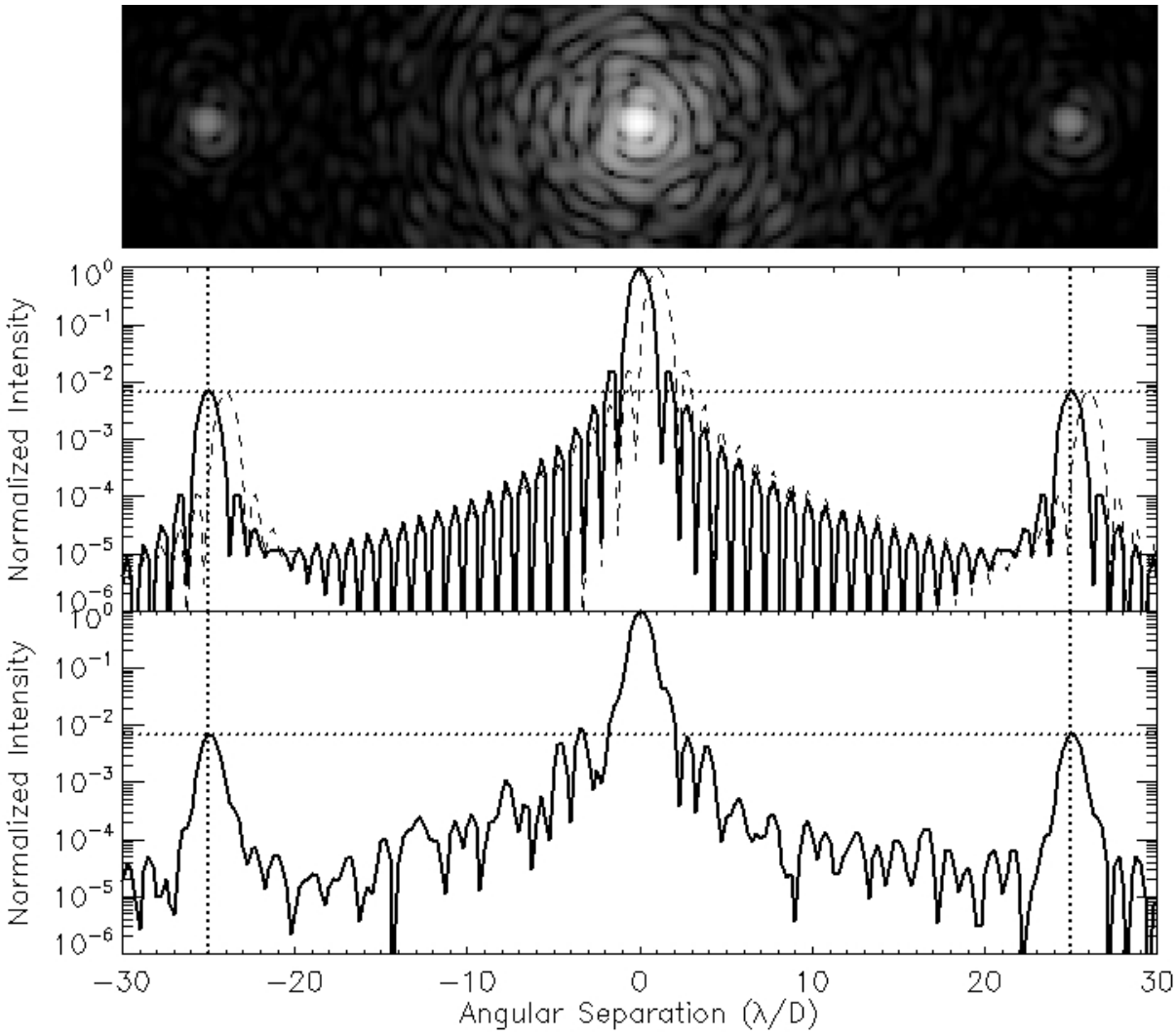

Fig. 2.— Same as Fig. 1 for an added amplitude sine wave mask.

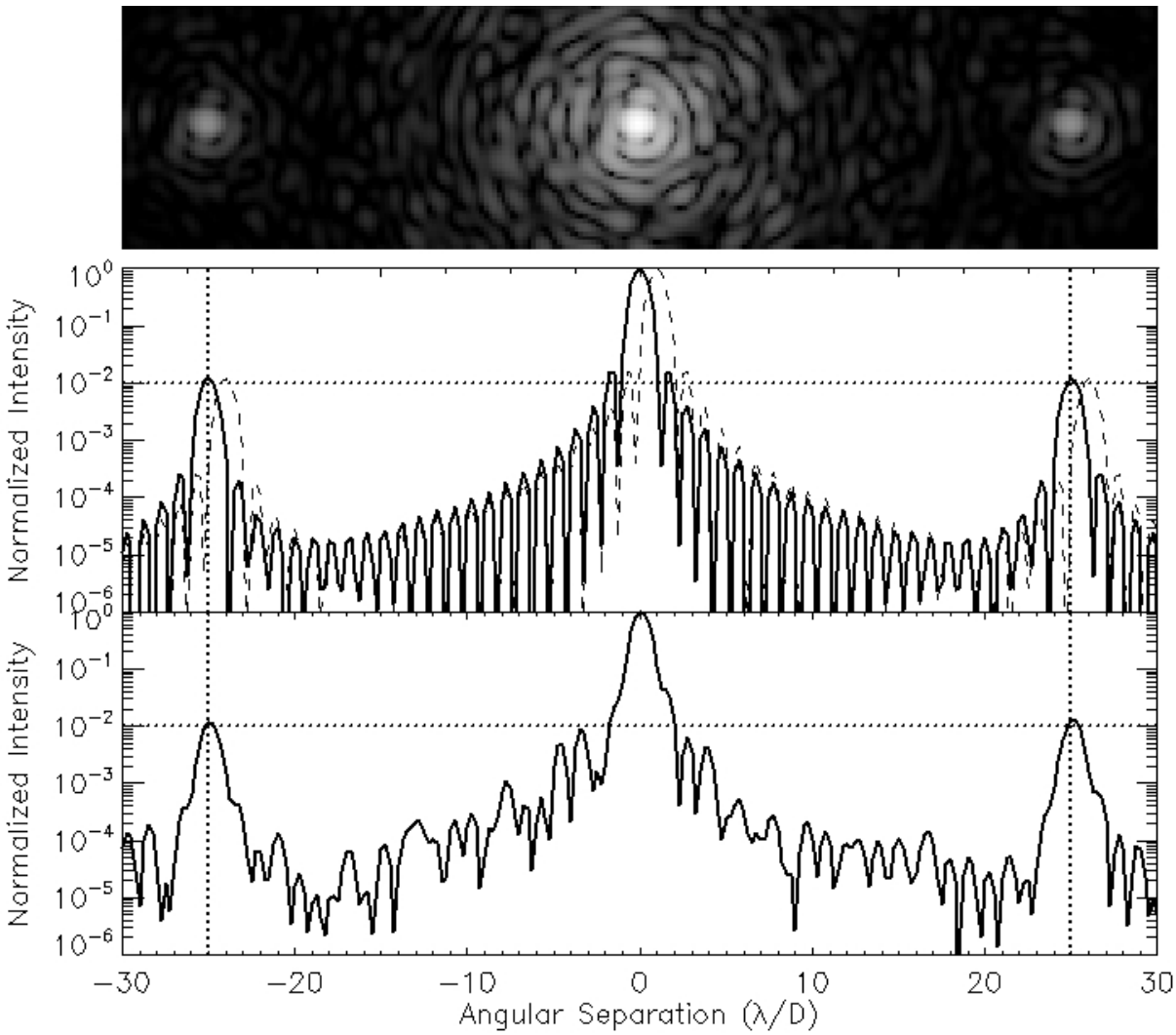

Fig. 3.— Same as Fig. 1 for an added transmissive amplitude grating. This figure shows the first two bright satellite PSFs. Numerous fainter satellite PSFs exist at wider separation.

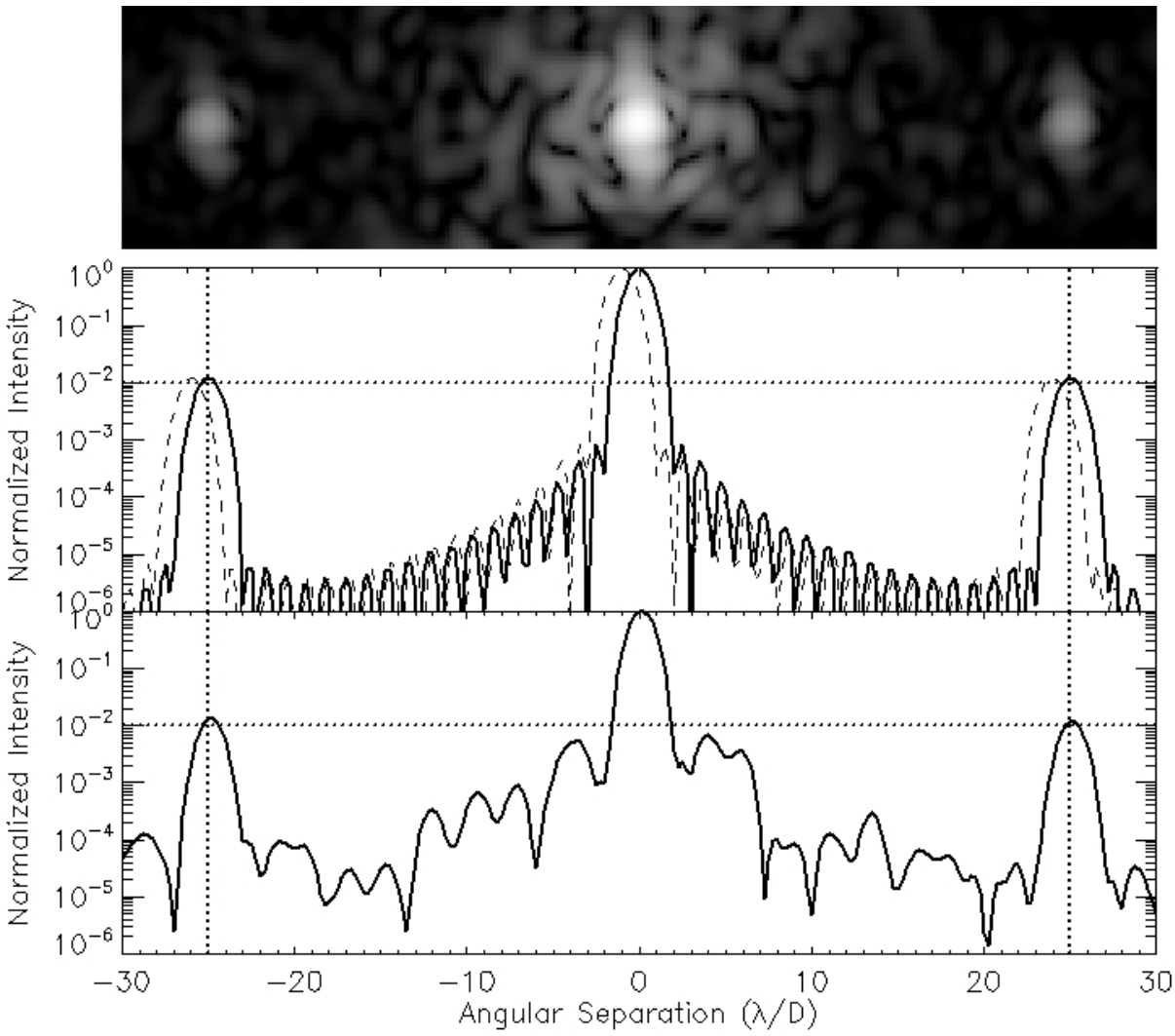

Fig. 4.— Same as Fig. 1 for an apodized pupil coronagraph with a transmissive amplitude grating.

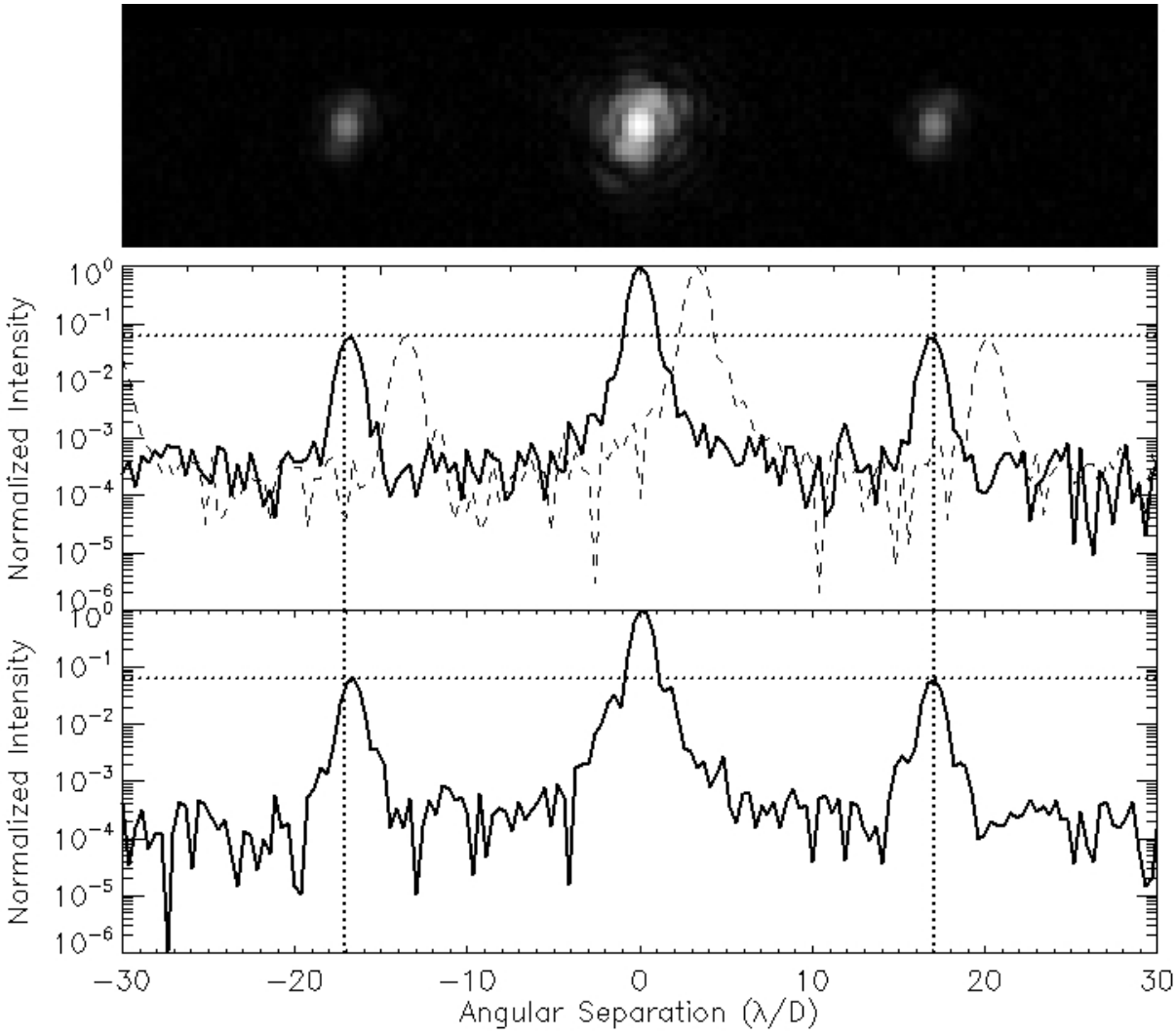

Fig. 5.— Same as Fig. 1 for the laboratory experiment using a transmissive amplitude grating.